Journal of Thermal Engineering
Yildiz Technical University Press, Istanbul, Turkey
Vol. 1, No. 1, pp. 42-60, January, 2015.

http://eds.yildiz.edu.tr/journal-of-thermal-engineering/Articles
Manuscript Received June 17, 2014; Accepted June 27, 2014

This paper was recommended for publication in revised form by Editor-in-Chief Ahmet Selim Dalkilic

NUMERICAL SIMULATION AND MATHEMATICAL ANALYSIS OF FLOW-WALL INTERACTION IN THE LARGE DEFORMATION DOMAIN: APPLICATION TO THE DYNAMICS OF THE ANEURYSMS

Mahmoud Hamadiche

LMFA, Ecole Centrale de Lyon, 36 Avenue Guy de Collongue, 69134, Ecully, France

Email: mahmoud.hammadich@gmail.com

ABSTRACT

A numerical method is derived to take account of full flow-wall interaction in la large deformation domain. To this end, a simplified Lagrangian and nonlinear model is derived to describe the wall motion. the flow is described by two dimensional Naiver stokes equation. The projection method is used to solve for the flow and fourth Rung-Kutta method is used to solve wall equation. The formulation of the problem allows full flow and wall interaction via the boundary conditions at the interface flow-wall. Some numerical simulation will be presented with periodic inlet flow.

The method is applied to study the dynamics of aneurysms in arteries and veins. The flow inside the aneurysm is examined under the effects of a steady inlet flow as well as a pulsatile inlet flow for different aneurysm sizes. The wall model is analyzed when the wall is subjected to a constant transmural pressure and a quasi uniform inviscid flow. For a steady constant transmural pressure, a formal solution of the non linear integral-partial differential equation governing the wall motion is derived. For a steady and a quasi uniform inviscid flow, a first integral of the wall equation is obtained, then the solution is found to satisfy an integral non linear equation which is solved by numerical iteration.

INTRODUCTION

The flow-wall interaction occurs in large number of practical applications, where the coupling between the flow and the moving machine components promotes the development and the creation of a coupled vibration. In energy domain these coupled vibrations arises in drill string, pipeline, compressor and turbine rotor-stator of natural gas compression installation for gas liquidization, valves of oil well and in offshore oil plate-form, the mentioned vibrations occur often in the small deformation domain but can reach large deformations domain and cause serious risk for the installation. In Aeronautic, elastic flexible panels are used as a control tool, B. H. Tan, A.D. Lucey and R. M. Howell [17], among others, studied the stability of a panel under a uniform flow subjected to an infinitesimal disturbance. The panel is supported by a continuous elastic foundation. Euler-Bernoulli beam model is used to describe the panel motion, while the flow is supposed to be irrational, thus the velocity is the gradient of a scalar function and the pressure is given by linearized Bernoulli theorem. The boundary elements method is used to reduce the initially two dimensional problem to one dimensional problem using the displacement of the panel as unknown variable. It is shown that the system becomes unstable if the speed of the flow exceeded some critical prescribed value. Two applications are addressed in their work, the interaction of the panel with water and the interaction of the panel with air. It is show that adding a stiffer spring in the mid-chord of the foundation of the panel delays the divergence instability. It is shown that increasing the stiffness of the spring beyond some critical value does not effect on the instability of the system

A drill string model is considered by O. Doaré and E. de Langre [15] where the stability of a hanging fluid-conveying pipe is investigated. The pipe is modeled as Bernoulli-Euler beam and the non viscous flow is uniform in the pipe cross section. It is concluded that the system become unstable when

the flow velocity exceeds some defined critical value. It is found that the threshold velocity depends on the length of the pipe, the threshold velocity decreases with the increase of the length of the pipe

Another example of flow wall interaction is considered by M. Hamadiche and H. Abou-Shady [16], where the stability of optic fiber coating system has been studied. In order to increase the flexural resistance of the optical fiber, they are usually coated by a resin. During the coating process, the fiber runs through a die filled by resin. Experimental evidences show that the coating system becomes unstable for highly traveling speed of the optical fiber. M. Hamadiche and H. Abou-Shady identified the origin of the instability of the system by studying the stability of the flowing resin in the die when coupled with a viscoelastic optical fiber. A numerical code based on the sixth order compact finite difference method is derived to solve the two-dimensional Navier-Stokes equations. It has been shown that the flow bifurcates for a given value of Reynolds number wherever the optical fiber vibration has been experimentally observed. The stability of the resulting flow coupled with a non-rigid optical fiber is analyzed. Two-dimensional and three-dimensional stability analysis was undertaken. The system was found to be subjected to two different kinds of instabilities induced by two unstable and distinguishable groups of modes. The predicted threshold optic fiber speed is in good agreement with experimental results.

M. Hamadiche and M. Gad-el-Hak studied the stability of the Hagen–Poiseuille flow of a Newtonian fluid in an incompressible, collapsible or non collapsible visco-elastic tupe using linear stability analysis. The dependence of the tube's diameter in the base state on the axial distance is explicitly accounted for in this formulation. A novel numerical strategy is introduced to study the spatio–temporal stability of the coupled fluid–structure system subjected to infinitesimal axisymmetric or non-axisymmetric disturbances. Axisymmetric disturbances correspond to the azimuthal wave number $n = 0$. There, they have identified two convective instability modes one propagating upstream and the other downstream. For each of the non-axisymmetric disturbances $n = 1 - 6$, they have found one absolute instability propagating upstream, while for $n = 1,2$, downstream-propagating convective modes are additionally observed. Two of the standing waves have equal frequencies at their respective cusp points, while a third absolute instability has triple that frequency, in good agreement with existing experiments. The $n = 1$ absolute instability mode is replaced by a convective mode when the Reynolds number exceeds 200, while the other standing waves, at $n =$ 2–6, persist to high Re values. Increasing the solid's viscosity, thickness or shear modulus causes the absolute instability modes to become convective as well as to ultimately become stable. M. Hamadiche, M. Gad-el-Hak and N. Kizilova [12] have shown that the absolute instability can be removed by changing the viscosity of the meddle layer of multilayered visco-elastic tube.

In bio-mechanic, the flow-wall interaction occurs in arteries, veins and in the heart where small and large displacement can be involved. The mentioned application are, of course, not exclusive. The numerical simulation of these sort of problems is very difficult due to the fact that both fluid domain and solid domain are time dependent. The time dependent domain requires that the numerical mesh be updated at each time step during numerical simulation. When the deformation and the displacement are smaller than the characteristic length scale of the considered problem, the technique of linearisation becomes helpful, and the problem can be reduced to a problem of time independent domain by linearisation of the boundary conditions at the fluid-solid interface. However, when large deformation and large displacement are involved, a careful analysis is needed to tackle the domain displacement and the nonlinear deformation associated with it.

An aneurysm is a blood-filled bulge in the wall of a blood vessel that commonly occurs in arteries at the base of the brain, and in the main artery carrying blood from the left ventricle of the heart. When the size of the aneurysm increases, there is a significant risk of rupture, resulting in severe hemorrhage, complications or death, a phenomena known as a stroke.

The aneurysms occur when part of a blood vessel inflates abnormally due to damage or a weakness in its wall. As the wall is weakened, it balloons out under the action of transmural pressure at its weakest point creating a saccular or fusiform bulge called aneurysm. As the aneurysm grows, the deformation and the displacement of the wall become large, the stress increases which leads to the rupture of the wall at the aneurysm. The aneurysm is likely to form as a result of a biological processes caused by biochemical or structural inherited defects, infection disease and specific hemodynamic factors [1]-[2]. The fact that the aneurysm often occurs at a specific location in arteries and veins, characterized by unique hemodynamic conditions, strongly suggests that the hemodynamic plays an important role in the formation and in the development of aneurysms [3].

The arterial and venous walls are composed of concentric layers with different thicknesses and mechanical properties [5]-[7]. The innermost layer, called intima, it consists of a mono-layer of endothelial cells. The endothelial cells are sensitive to shear stress and pressure exerted by the blood flow at the wall. The intima contributes insignificantly to the mechanical property

of the arterial wall. The middle layer, the media, is responsible for most of mechanical properties of arteries. The media consists of a complex three-dimensional network of elastin and collagen fibers, smooth muscle cells and proteoglycans. The outermost layer is called adventitia. It consists of thick bundles of collagen fibers, some elastin fibers, fibroblasts, nerves and an intravascular bed. The adventitia influences the mechanical properties mainly by facilitating tethering to the surrounding tissue and by limiting the lumen increase and damage of the vessel at high transmural pressures. Media and adventitia can be considered as fiber-reinforced composites due to the helical structure formed by the collagen microfibrils [7]. The abdominal aortic aneurysm is characterized by a marked deterioration of the media layer, which results in a significant increase in collagen fibers and significant decrease in elastin fibers. It is suggested that, in abdominal aorotic aneurym, elastin degradation is likely to occur in the region of low shear stress [8].

Several nonlinear mathematical models describing the long term evolution of aneurysms have been developed in, among others, [7], [8] and [9]. In those models, the replacement rate of elastin fibers by collagen fibers is supposed to be dependent on hemodynamic conditions. As the time scale of the dynamics considered by these models, which is of the order of several years, is very large in comparison of the heart cycle, which is of the order of one second, the hemodynamic conditions (pressure and stress) are found by solving the Navier-Stokes equations in a fixed domain. The fixed domain is updated every once in a while to take account to the evolution of the geometry of the aneurysm. Therefore, the movement of the wall implicitly supposed not affect the flow. The present work is mainly concerned by the action of the movement of the wall on the flow and vice versa; therefore, a full interaction between the flow and the wall is considered. In order to build a tractable model allowing full flow-wall interaction we opted for a simplified equation governing the wall motion. Nevertheless, the obtained equation preserves the main feature of aneurysm wall, namely, geometrical non linearity. To this end, a mathematical model using Lagrangian representation and describing the aneurysm's wall motion is presented, then a numerical simulation, taking into account a full coupling between the blood flow and the motion of the wall of the aneurysm, is performed.

The flow-wall interaction occurs in a large number of practical applications and theoretical formulation of many important problems. The numerical simulation of this type of problems is very difficult, for both the fluid domain and the solid domain evolve. The time-dependent domain requires that the numerical mesh must be updated at each time step during a numerical simulation. When the deformation and the displacement are smaller than the characteristic length of the considered problem, the technique of linearization becomes helpful, and the problem can be reduced to a problem of time-independent domains. However, when large deformation and large displacement are involved, a careful analysis is needed to tackle the domain displacement and to compute the large deformation. A typical problem, where large displacement and large deformation in flow-wall coupled dynaminc occur, is the abdominal aortic aneurysm, a common vascular disease among the adult population.

The interaction between a non rigid wall and the flow often leads to an unstable system [12], [14] and the nature of these instabilities is absolute one [13]. In many engineering problems the displacement of the wall during its interaction with the flow is large enough to invalidate linear approximation of the governing partial differential, as can be concluded from the experimental work of [10] and theoretical analysis of [18]. The nonlinearity in the soft solid part of the system can be geometrical, induced by a large displacement of the wall, and can be rheological resulting from the nonlinear stress-train relation. The two mentioned nonlinearity can of course coexist. The work presented here focuses on geometrical nonlinearity. Another nonlinearity arises when the Reynolds number of the flow is large enough for fluid inertial forces to dominate over fluid viscous forces far from the wall. This nonlinearity is taken into account here. The problem is formulated as follows: the motion of the wall is described using Lagrangian variables while the flow is described by Eulerian variables. The formulation yields a nonlinear integral partial differential equation governing the wall motion. The solution of the wall equation is discussed in some peculiar cases in order to validate the wall model. In sections 2 and 3 the wall equation is derived. Section 4 presents the flow equation used in the numerical simulation. Sections 5, 6 and 7 present the numerical method and numerical results respectively. Analysis of the wall model is presented in section 8, 9 and 10. A conclusion is given in section 11.

2 LAGRANGIAN KINEMATICAL DESCRIPTION OF THE WALL

We consider an incompressible continuum where displacements in the a_1 and a_2 directions are allowed. The continuum is observed in a frame of reference $R=(0,a_1,a_2,a_3)$ having the vectors (x_1,x_2,x_3) as an orthonormal basis, as sketched in figure 1. The variables a_1, a_2, a_3 are Lagrangian variables describing the reference state of the wall, which is a plane shell of thickness h. In order to have a simplified governing equation for the motion

of the wall, the displacement is assumed to depend only on a_1 and on time t. Assuming the previous assumption is valid, the tensor gradient of deformation can be calculated:

$$\mathbf{F} = \begin{pmatrix} 1+\frac{\partial u_1}{\partial a_1} & 0 & 0 \\ \frac{\partial u_2}{\partial a_1} & 1 & 0 \\ 0 & 0 & 1 \end{pmatrix}$$

In the case where the continuum is incompressible, which henceforth is assumed, the condition det (F) = 1 has to be enforced, which yields $\frac{\partial u_1}{\partial a_1}=0$. The aneurysm considered here is assumed to be tethered at its staring point to a rigid wall, i.e. the displacement of the wall of the healthy artery is assumed to be small in comparison to the displacement of the wall of the aneurysm. Then the non displacement condition at the aneurysm starting point requires that $u_1=0$ and the tensor gradient of deformation becomes

$$\mathbf{F} = \begin{pmatrix} 1 & 0 & 0 \\ \frac{\partial u_2}{\partial a_1} & 1 & 0 \\ 0 & 0 & 1 \end{pmatrix}$$

Therefore, the deformation tensor can be written as

$$\mathbf{X} = \tfrac{1}{2}(\mathbf{F}^{\mathrm{T}}\mathbf{F} - \mathbf{I}) = \tfrac{1}{2}\begin{pmatrix} (\frac{\partial u_2}{\partial a_1})^2 & \frac{\partial u_2}{\partial a_1} & 0 \\ \frac{\partial u_2}{\partial a_1} & 0 & 0 \\ 0 & 0 & 0 \end{pmatrix}$$

Let $\hat{\hat{\sigma}}$ be the second Piola-Kirchhoff tensor, a linear strain stress dependency can be assumed and a constitutive equation can be sought in the form:

$$\hat{\hat{\sigma}} = -p\mathbf{I} + 2\mu\mathbf{X} = -\begin{pmatrix} p & 0 & 0 \\ 0 & p & 0 \\ 0 & 0 & p \end{pmatrix} + \mu\begin{pmatrix} (\frac{\partial u_2}{\partial a_1})^2 & \frac{\partial u_2}{\partial a_1} & 0 \\ \frac{\partial u_2}{\partial a_1} & 0 & 0 \\ 0 & 0 & 0 \end{pmatrix}$$

where μ is the viscosity coefficient. Let $\hat{\sigma} = \mathbf{F}\hat{\hat{\sigma}}$ be the first Piola-Kirchhoff tensor, thus,

$$\hat{\sigma} = -p\begin{pmatrix} 1 & 0 & 0 \\ \frac{\partial u_2}{\partial a_1} & 1 & 0 \\ 0 & 0 & 1 \end{pmatrix} + \mu\begin{pmatrix} 1 & 0 & 0 \\ \frac{\partial u_2}{\partial a_1} & 1 & 0 \\ 0 & 0 & 1 \end{pmatrix}\begin{pmatrix} (\frac{\partial u_2}{\partial a_1})^2 & \frac{\partial u_2}{\partial a_1} & 0 \\ \frac{\partial u_2}{\partial a_1} & 0 & 0 \\ 0 & 0 & 0 \end{pmatrix}$$

which yields.

$$\hat{\sigma} = -\begin{pmatrix} p & 0 & 0 \\ \frac{\partial u_2}{\partial a_1}p & p & 0 \\ 0 & 0 & p \end{pmatrix} + \mu\begin{pmatrix} (\frac{\partial u_2}{\partial a_1})^2 & \frac{\partial u_2}{\partial a_1} & 0 \\ (\frac{\partial u_2}{\partial a_1})^3 + \frac{\partial u_2}{\partial a_1} & (\frac{\partial u_2}{\partial a_1})^2 & 0 \\ 0 & 0 & 0 \end{pmatrix}$$

The above equation shall be used in the momentum equation of the wall in the next section.

3 SHELL'S MOMENTUM EQUATION

The Lagrangian representation for momentum equation governing the motion of a deformable continuum, following [11], is

$$\rho\frac{\partial^2\mathbf{u}}{\partial t^2} = \rho\mathbf{f} + div(\hat{\sigma}) \qquad (1)$$

where u is the displacement vector, ρ is the mass density in the reference state, f is the density of external forces which shall be neglected later and $\hat{\sigma}$ is the first Piola-Kirchhoff tensor. Let a slice of the shell be enclosed in the interval a_1 and a_1+da_1 and let h be the thickness of the shell in the reference state. The integration of the momentum equation over the volume of the slice yields

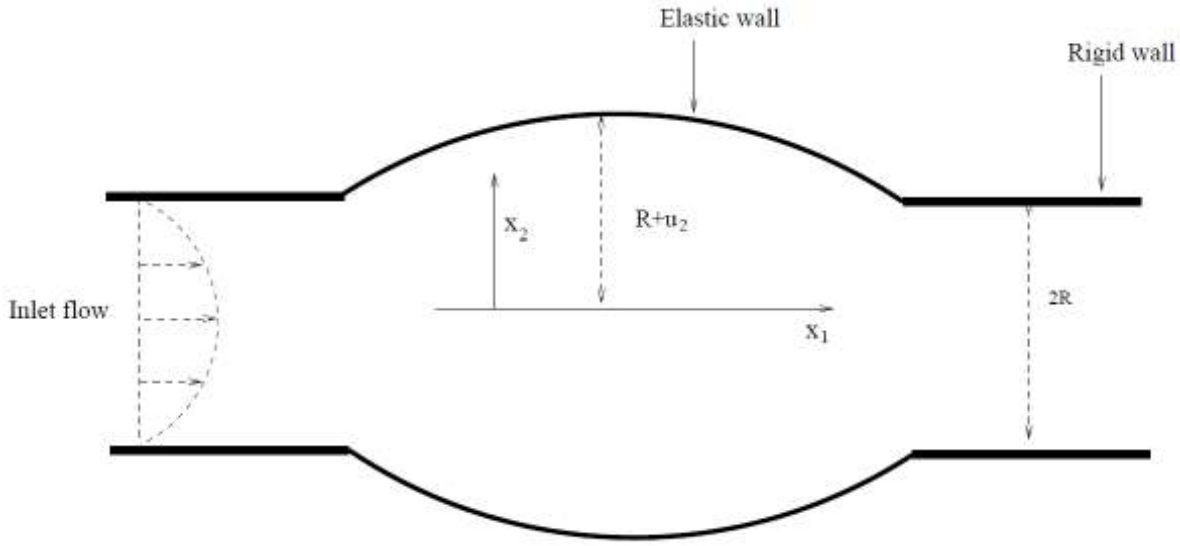

Figure 1: Schematic representation of the aneurysm

$$h\rho\frac{\partial^2\mathbf{u}}{\partial t^2}da_1da_3 = \int_{a_1+da_1}\hat{\boldsymbol{\sigma}}\cdot\mathbf{x}_1da_2da_3 - \int_{a_1}\hat{\boldsymbol{\sigma}}\cdot\mathbf{x}_1da_2da_3 + \int_{a_2+h}\hat{\boldsymbol{\sigma}}_e\cdot\mathbf{x}_2da_1da_3 - \int_{a_2}\hat{\boldsymbol{\sigma}}_i\cdot\mathbf{x}_2da_1da_3, \quad (2)$$

$\hat{\sigma}_e$ and $\hat{\sigma}_i$ stand for the first Piola-Kirchhoff tensor at the exterior and at the interior shell surfaces respectively. Taking into account equation 1, the above equation becomes

$$h\rho\frac{\partial^2\mathbf{u}}{\partial t^2}da_1da_3 = h\frac{\partial(\hat{\boldsymbol{\sigma}}\cdot\mathbf{x}_1)}{\partial a_1}da_1da_3 + (\hat{\boldsymbol{\sigma}}_e - \hat{\boldsymbol{\sigma}}_i)\cdot\mathbf{x}_2da_1da_3$$

therefore, the simplified version of the equation of motion of the shell can be written as

$$\rho\frac{\partial^2\mathbf{u}}{\partial t^2} = \frac{\partial(\hat{\boldsymbol{\sigma}}\cdot\mathbf{x}_1)}{\partial a_1} + \frac{1}{h}(\hat{\boldsymbol{\sigma}}_e - \hat{\boldsymbol{\sigma}}_i)\cdot\mathbf{x}_2$$

The explicit form of the first term in the right hand side is

$$\hat{\boldsymbol{\sigma}}\cdot\mathbf{x}_1 = \begin{pmatrix} -p+\mu(\frac{\partial u_2}{\partial a_1})^2 \\ -p\frac{\partial u_2}{\partial a_1} + \nu(\frac{\partial u_2}{\partial a_1})^3 + \mu\frac{\partial u_2}{\partial a_1} \\ 0 \end{pmatrix},$$

$$\frac{\partial(\hat{\boldsymbol{\sigma}}\cdot\mathbf{x}_1)}{\partial a_1} = \frac{\partial}{\partial a_1}\begin{pmatrix} -p+\mu(\frac{\partial u_2}{\partial a_1})^2 \\ -p\frac{\partial u_2}{\partial a_1} + \nu(\frac{\partial u_2}{\partial a_1})^3 + \mu\frac{\partial u_2}{\partial a_1} \\ 0 \end{pmatrix}$$

In order to compute the second term on the right hand side of equation 4, we recall that Newton's third law implies that

$$\boldsymbol{\sigma}\cdot\mathbf{n}ds = \boldsymbol{\sigma}_f\cdot\mathbf{n}ds \text{ ; at the interface fluid/solid,} \quad (5)$$

where σ and σ_f are the Cauchy stress tensor in the solid and in the fluid, respectively. According to [11]**Error! Reference source not found.**, the surface element in the reference state can be mapped onto the surface element in actual stat according to

$$\mathbf{n}ds = \mathbf{G}^T\cdot\mathbf{n}_0ds_0 \quad (6)$$

where the subscript 0 stands for the quantity in the reference state of the solid continuum, and G is the inverse of the tensor of gradient of deformation F , and G^T is the transpose of G , that is,

$$\mathbf{G}^T = \begin{pmatrix} 1 & -\frac{\partial u_2}{\partial a_1} & 0 \\ 0 & 1 & 0 \\ 0 & 0 & 1 \end{pmatrix} \quad (7)$$

Substituting equation 6 into equation 1 yields

$\sigma . G^T . n_0 ds_0 = \sigma_f . G^T . n_0 ds_0$;at the interface fluid/solid (8)

Knowing that in incompressible material, the first Piola-Kirchhoff is by definition

$$\hat{\boldsymbol{\sigma}} = \boldsymbol{\sigma} \cdot \mathbf{G}^T \tag{9}$$

equation 8 becomes

$$\hat{\boldsymbol{\sigma}} \cdot \mathbf{n}_0 ds_0 = \boldsymbol{\sigma}_f \cdot \mathbf{G}^T \cdot \mathbf{n}_0 ds_0 \tag{10}$$

at the interface fluid/solid. In an inviscid fluid the Cauchy stress tensor is

$$\boldsymbol{\sigma}_f = -p_f \mathbf{I} \tag{11}$$

Henceforth the axial shear stress at the interface solid/fluid shall be neglected in the solid model as the model written in this paper prohibits the axial displacement of solid particles. Taking into account the fact that n_0 is the normal to the surface of the shell in the reference state, it must be identified as x_2. Let p_e and p_i stand for the outside and the inside fluid pressure respectively, then equation 10 becomes

$$\hat{\boldsymbol{\sigma}}_e \cdot \mathbf{x}_2 = -p_e \mathbf{G}^T \cdot \mathbf{x}_2 \tag{12}$$

at the outside interface fluid/solid, and

$$\hat{\boldsymbol{\sigma}}_i \cdot \mathbf{x}_2 = -p_i \mathbf{G}^T \cdot \mathbf{x}_2 \tag{13}$$

at the outside interface fluid/solid. Substituting equation 7 into the precedent equations, we have

$$\hat{\boldsymbol{\sigma}}_e \cdot \mathbf{x}_2 = \begin{pmatrix} p_e \frac{\partial u_2}{\partial a_1} \\ -p_e \\ 0 \end{pmatrix} \; ; \; \begin{pmatrix} \hat{\boldsymbol{\sigma}}_i \cdot \mathbf{x}_2 = \\ p_i \frac{\partial u_2}{\partial a_1} \\ -p_i \\ 0 \end{pmatrix}$$

Substituting these equations into equation 4 yields

$$\rho \begin{pmatrix} \frac{\partial^2 u_1}{\partial t^2} \\ \\ \frac{\partial^2 u_2}{\partial t^2} \end{pmatrix} = \begin{pmatrix} -\frac{\partial p}{\partial a_1} + \mu \frac{\partial}{\partial a_1}[(\frac{\partial u_2}{\partial a_1})^2] + \frac{p_e - p_i}{h} \frac{\partial u_2}{\partial a_1} \\ \\ \rho \begin{pmatrix} 0 \\ \\ \frac{\partial^2 u_2}{\partial t^2} \end{pmatrix} = \end{pmatrix}$$

$$\begin{pmatrix} -\frac{\partial p}{\partial a_1} + \mu \frac{\partial}{\partial a_1}[(\frac{\partial u_2}{\partial a_1})^2] + \frac{p_e - p_i}{h} \frac{\partial u_2}{\partial a_1} \\ \\ -\frac{\partial}{\partial a_1}(p \frac{\partial u_2}{\partial a_1}) + \mu \frac{\partial}{\partial a_1}[(\frac{\partial u_2}{\partial a_1})^3 + \frac{\partial u_2}{\partial a_1}] - \frac{p_e - p_i}{h} \end{pmatrix}$$

The first equation could be integrated to get an explicit formal solution for the pressure inside the shell, that is

$$p = \mu(\frac{\partial u_2}{\partial a_1})^2 + \int_0^{a_1} \frac{p_e - p_i}{h} \frac{\partial u_2}{\partial \eta} d\eta + \chi \tag{14}$$

χ is an arbitrary constant. The integration constant stands for the tension inside the shell in the state of reference. In an unstressed shell in the state of reference, the constant is zero. It is positive for a compressed shell in the state of reference and, it is negative for a stretched shell in the state of reference. In this work the constant is set to zero. Multiplying the the preceding equation by $\frac{\partial u_2}{\partial a_1}$ and taking the derivative with respect to a_1 yields

$$\frac{\partial}{\partial a_1}[p \frac{\partial u_2}{\partial a_1}] = \mu \frac{\partial}{\partial a_1}[(\frac{\partial u_2}{\partial a_1})^3] + \frac{\partial^2 u_2}{\partial a_1^2} \int_0^{a_1} \frac{p_e - p_i}{h} \frac{\partial u_2}{\partial \eta} d\eta + (\frac{\partial u_2}{\partial a_1})^2 \frac{p_e - p_i}{h} \tag{15}$$

substituting this equation in the second momentum equation, i.e. the second equation of the set of equations number 14, leads to

$$\rho \frac{\partial^2 u_2}{\partial t^2} = +\mu \frac{\partial}{\partial a_1}[(\frac{\partial u_2}{\partial a_1})^3 + \frac{\partial u_2}{\partial a_1}] - \frac{p_e - p_i}{h} - \mu \frac{\partial}{\partial a_1}[(\frac{\partial u_2}{\partial a_1})^3] - \frac{\partial^2 u_2}{\partial a_1^2} \int_0^{a_1} \frac{p_e - p_i}{h} \frac{\partial u_2}{\partial \eta} d\eta - (\frac{\partial u_2}{\partial a_1})^2 \frac{p_e - p_i}{h} \tag{16}$$

After simplification, the integral-partial differential equation describing the wall motion can be written as

$$\rho \frac{\partial^2 u_2}{\partial t^2} = \mu \frac{\partial^2 u_2}{\partial a_1^2} - \frac{\partial^2 u_2}{\partial a_1^2} \int_0^{a_1} \frac{p_e - p_i}{h} \frac{\partial u_2}{\partial \eta} d\eta - [(\frac{\partial u_2}{\partial a_1})^2 + 1] \frac{p_e - p_i}{h} \tag{17}$$

4 BASIC FLOW EQUATIONS

The flow is modeled by the two dimensional Navier-Stokes equations for incompressible and viscous fluid with mass density ρ_f and kinematic viscosity ν, that is,

$$\frac{\partial \mathbf{v}}{\partial t} + \mathbf{v} \cdot \nabla \mathbf{v} = -\nabla p + \nu \Delta \mathbf{v} \tag{18}$$

$$\nabla \cdot \mathbf{v} = 0 \tag{19}$$

where v is the velocity vector, p is the pressure to density ratio, $\nabla = \left(\frac{\partial}{\partial x}, \frac{\partial}{\partial y}\right)$ is the gradient operator and $\Delta = \frac{\partial^2}{\partial x^2} + \frac{\partial^2}{\partial y^2}$ is the Laplacian operator. The flow equations are subjected to the boundary conditions

$$v = u_1^0(y)x_1; \text{ at the inlet of the channel} \tag{20}$$

where $u_1^0(y)$ is a known function which shall be introduced explicitly later and x_1 is the unit vector parallel to the channel axis.

$$\frac{\partial v}{\partial x} = 0;\ p = p_0; \text{ at the exit of the channel} \tag{21}$$

p_0 is a given outlet pressure.

$$v = 0; \text{ at the rigid solid wall} \tag{22}$$

$$v = \frac{\partial u_2}{\partial t} x_2; \text{ at the elastic wall} \tag{23}$$

The function u_1^0 involved in the inlet flow is

$$u_1^0 = u_0[1 - (\frac{y}{R})^2](\alpha_1 + \alpha_2 F) \tag{24}$$

u_0 is constant of $o(1)$ and

$$\begin{gathered} F = \alpha \frac{\delta^k}{(\gamma + \delta^k)^3}[(1 + e^{\beta})] \ ; \ \beta = \frac{2\sin(2\pi\omega t)}{\sigma^2} \\ \delta = 2\pi(t - t_n) \ ; \ t_n \le t < t_{n+1} \\ t_n = 2\pi n \ ; \ n \in \{0, 1, 2, \cdots\} \end{gathered} \tag{25}$$

and, unless otherwise stated,

$$\alpha = 3 \ ; \ k = 4 \ ; \ \gamma = 1 \ ; \ \sigma = 1 \ ; \ \omega = 1 \tag{26}$$

The numerical simulation of the flow is difficult with a moving boundary. To overcome this difficulty, the physical domain is mapped onto a rectangular one using the following coordinates transformation:

$$t = \tau \ ; \ X = x \ ; \ Y = \frac{y}{R + \xi(x,t)} \ ; \ y \ge 0 \tag{27}$$

upper elastic wall. In a similar way a new variable are introduced for $y < 0$, that is

$$t = \tau \ ; \ X = x \ ; \ Y = \frac{y}{R + \eta(x,t)} \ ; \ y \le 0 \tag{28}$$

where $\eta(x,t) = -u_2$, and u_2 is the displacement of the lower elastic wall. The derivative rule is applied to compute all the derivatives involved in Navier-Stokes equations, namely,

$$\frac{\partial}{\partial t} = \frac{\partial}{\partial \tau} - \frac{\partial \xi(X,\tau)_n}{\partial \tau}[R + \xi(X,\tau)]^{-1} Y \frac{\partial}{\partial Y} \tag{29}$$

$$\frac{\partial}{\partial x} = \frac{\partial}{\partial X} - \frac{\partial \xi(X,\tau)}{\partial X}[R + \xi(X,\tau)]^{-1} Y \frac{\partial}{\partial Y} \tag{30}$$

$$\frac{\partial}{\partial y} = [R + \xi(X,\tau)]^{-1} \frac{\partial}{\partial Y} \tag{31}$$

Similar expressions for the lower wall can be written in an analogous manner.

5 NUMERICAL METHOD USED FOR WALL EQUATION

Once the interior pressure p_i and external pressure p_e are known, equation 17 are solved numerically. The time derivative is evaluated using a second order finite difference scheme, thus

$$(\frac{\partial^2 u}{\partial t^2})^n = \frac{u^{n+1} - 2u^n + u^{n-1}}{\Delta t^2} \tag{32}$$

such that the discretised equation can be written as

$$\begin{aligned} \rho \frac{u^{n+1} - 2u^n + u^{n-1}}{\Delta t^2} = \\ \mu \frac{\partial^2 u_2}{\partial a_1^2} \Big|^{n+1} - \frac{\partial^2 u_2}{\partial a_1^2} \Big|^{n+1} \int_0^{a_1} \frac{p_e - p_i}{h} \Big|^n \frac{\partial u_2}{\partial \eta} \Big|^{n+1} d\eta \\ -[(\frac{\partial u_2}{\partial a_1} \Big|^{n+1})^2 + 1] \frac{p_e - p_i}{h} \Big|^n \end{aligned} \tag{33}$$

A numerical procedure based on a fourth order Range-Kutta method coupled with a shooting method is used to solve this equation. A similar procedure is developed for the other wall. The internal pressure p_i in vicinity of each wall is provided by numerical solution of the Poisson equation in the fluid domain. The external pressure is maintained constant.

6 NUMERICAL METHOD USED FOR FLUID EQUATIONS

A pressure-correction scheme (splitting method) is used to solve the two dimensional Navier-Stokes equations for incompressible fluid flow. A third-order time accurate scheme is used to evaluate the time derivative, namely,

$$(\frac{\partial \mathbf{v}}{\partial t})^{n+1} = \frac{3\mathbf{v}^{n+1} - 4\mathbf{v}^{n} + \mathbf{v}^{n-1}}{2\Delta t} \quad (34)$$

Euler first order scheme has been also tested, and the results obtained by the two schemes are in good agreement. The results shown here are obtained with third order method. The predictor step is

$$\frac{3\mathbf{v}^{*} - 4\mathbf{v}^{n} + \mathbf{v}^{n-1}}{2\Delta t} = -\mathbf{v}^{n} \cdot \nabla \mathbf{v}^{n} + Re^{-1}\Delta \mathbf{v}^{n} \quad (35)$$

v^* is the predictor velocity which is not divergence free, $Re = \frac{V_r \mathcal{L}}{\nu}$ is the Reynolds number, ν is the kinematic viscosity, V_r and $\mathcal{L}$ are the reference velocity and the reference length scales. In equation 35, the nonlinear terms are evaluated using first order up wind method and the viscous terms are evaluated using a second order finite difference method. The second step is to correct the predictor velocity v^*, such that the final obtained velocity is divergence free. In order to mantain the Navier-Stokes equations as the basic flow equations, the pressure has to satisfy the following equation,

$$\frac{3\mathbf{v}^{n+1} - 3\mathbf{v}^{*}}{2\Delta t} = -\nabla p \quad (36)$$

The flow velocity is sought to be divergence free, i.e. $\nabla \cdot v^{n+1} = 0$; therefore, the pressure is obtained by solving the Poisson equation:

$$\nabla \cdot \frac{3\mathbf{v}^{*}}{2\Delta t} = \Delta p \quad (37)$$

The gradient conjugate method is used to solve Poisson equation with the following boundary conditions

$\frac{\partial p}{\partial x} = 0$; at the inlet of the channel, (38)

$p = p_0$; at the exit of the channel, (39)

and

$n \cdot \nabla p = 0$; at solid and elastic wall, (40)

Finally, the divergence free flow velocity can be obtained from equation 36, that is

$$\mathbf{v}^{n+1} = \mathbf{v}^{*} - \frac{2}{3}\Delta t \nabla p \quad (41)$$

7 NUMERICAL RESULTS

In this section we shall show some numerical results such that the discretized equation can be written as presented are for steady inlet flow with curve and rigid wall, steady inlet flow with elastic wall and pulsatile inlet flow with elastic wall. In all cases, the constants involved in the definition of F in equation 25, are such that $a = a_1 = a_2 = 1$, $\gamma = 1$, $w = 1$ and $k = 3$ unless stated otherwise.

7.1 STEADY INLET FLOW WITH RIGID WALL

In order to examine the effect of the curvature of the wall, some numerical experiments have been done with a fixed wall and steady inlet flow, that is $a_2 = 0$ which cancels the unsteady part of the inlet flow. The transmural pressure to fluid density ratio is 10, i.e. $\frac{\Delta p}{\rho} = 10m^2/s^2$. A steady flow is obtained for the mentioned control parameters. Figure 2a shows the streamline for Reynolds number $Re = 1500$, and figure 2b shows streamlines for Reynolds number $Re = 2000$. Both figures show that the flow is quasi symmetric with two rolls located under the curve wall. The presence of rolls here is not surprising as the flow take place in a divergent-convergent channel. The flow in divergent or convergent channel bears the name of Jeffery-Hamel flow. The main feature of Jeffery-Hamel flow is the presence of symmetric rolls for a low Reynolds number regime and antisymmetric rolls for a high Reynolds number regime [4]. Numerical experiments performed for larger Reynolds number, $Re = 2500$ and $Re = 3000$, show that the flow has the same features as these shown in figures 2a and 2b, but the rolls are larger than those shown in figure 2a and 2b.

7.2 STEADY INLET FLOW WITH ELASTIC WALL

In this subsection the inlet flow is steady, i.e. $a_2 = 0$, which cancels the unsteady part of the inlet flow, while the curved part of the wall is elastic and can move under the action of transmural pressure. In this case the flow exhibits some unsteadiness, yet the wall displacement is very small in comparison to the width of the channel, and the change in

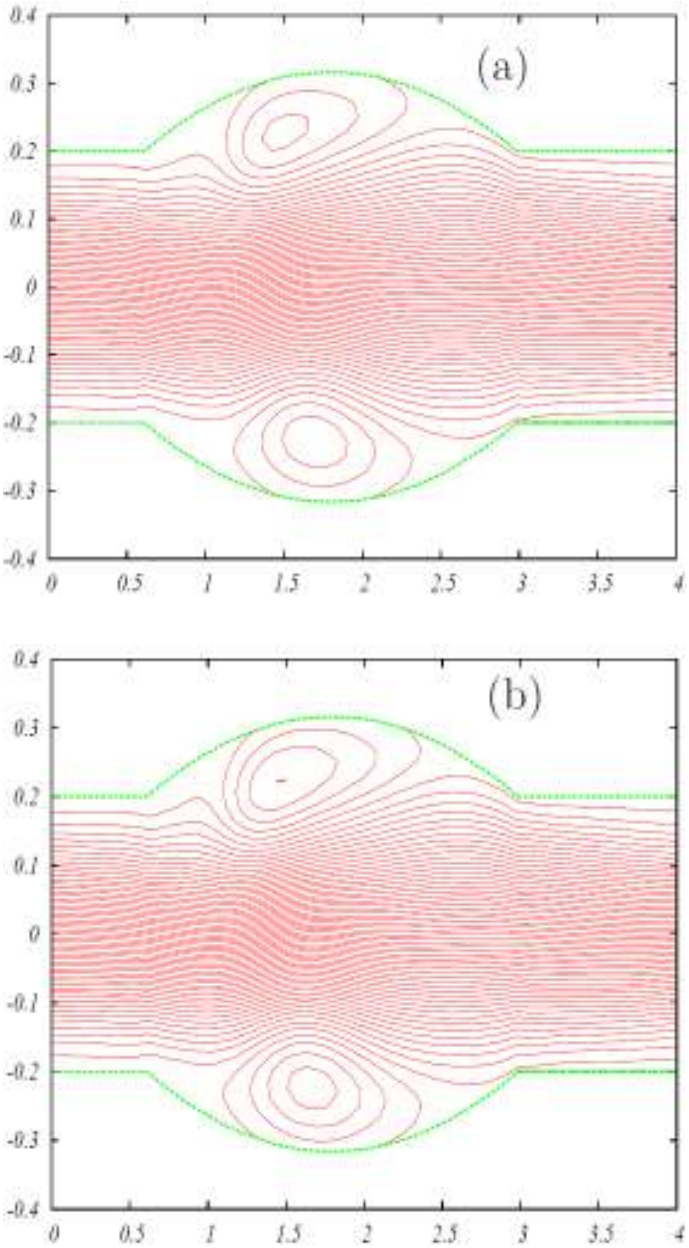

Figure 2: Steady streamlines obtained with curve rigid wall and steady inlet flow. (a) Reynolds number Re = 1500, (b) Reynolds number Re = 2000

streamlines over time is very small. Figures 3a-3b show the streamlines for Reynolds number $Re = 2000$ and $Re = 3000$, respectively, for a transmural pressure to fluid density ratio $\frac{\Delta p}{\rho} = 10m^2/s^2$. The figures show that the flow is asymmetric, a well known feature of Jeffery-Hamel flow in divergent channels [4]. Figures 3c-3d show the streamlines for Reynolds number $Re = 1500$ and $Re = 2000$, respectively, and for transmural pressure to fluid density $\frac{\Delta p}{\rho} = 15m^2/s^2$. As expected, the large transmural pressure outspreads the wall and allows larger rolls to be developed in the divergent-convergent part of the channel. Other numerical experiments, which are not shown here, show that for moving wall the flow remains asymmetric even for low Reynolds number regimes. Keeping in mind the main features of Jeffery-Hamel flow in a divergent channel, which can be symmetric or antisymmetric, the author has no explanation as why the asymmetric solution in figures 3a and 3b has benn selected thought the wall displacement is very small, while in a fixed wall the flow is quasi symmetric as it has been shown in figures 2a and 2b. However, it may be that the small displacement creates a small perturbation which causes the bifurcation from a symmetric to an asymmetric solution.

7.3 PULSATILE INLET FLOW WITH ELASTIC WALL

In order to simulate as much as possible the flow in arteries with the presence of an aneurysm, a combination of a pulsatile flow and a steady flow is used at the inlet of the channel. That is $a_1 = 1$ and $a_2 = 0.5$. It is found that, after a period long enough for the effects of the initial condition to have diminished, the flow reaches a periodic state, as is shown in figure 4. Figures 4a-4f show respectively, the function F, the axial velocity component, the lower wall displacement, the upper wall displacement, the pressure and the membrane tension at the center of the channel. In order to examine the flow during a cycle, eight stations are selected where the streamline of the flow are plotted. The + signs in figure 5 indicate the station in the dimensionless time interval [18-19]. Figures 6a and 6b taken at the stations (a) and (b) show the streamlines obtained when the flow reaches a steady state between two pulses, and this steady flow is rather asymmetric. Figures 6c and 6d show that the flow tend to be unidirectional in the systolic period, in that the two rolls present in the flow have been virtually disappeared in figures 6d-6f. For some other numerical experiments, which are not shown here, the rolls disappeared at the station (e). The largest wall displacement occurs at station (e) as seen in figure 6e. Surprisingly, the largest wall displacement takes place at station (e) where the inlet flow is not maximum, i.e. there is a delay in the wall response to the increase in flow rate. Figures 6g and 6h show that the flow reaches steady state again at the end of the period. Figure 7 show the streamlines of the flow in the same stations at a higher pressure to density ratio, i.e. $\frac{\Delta p}{\rho} = 15m^2/s^2$.

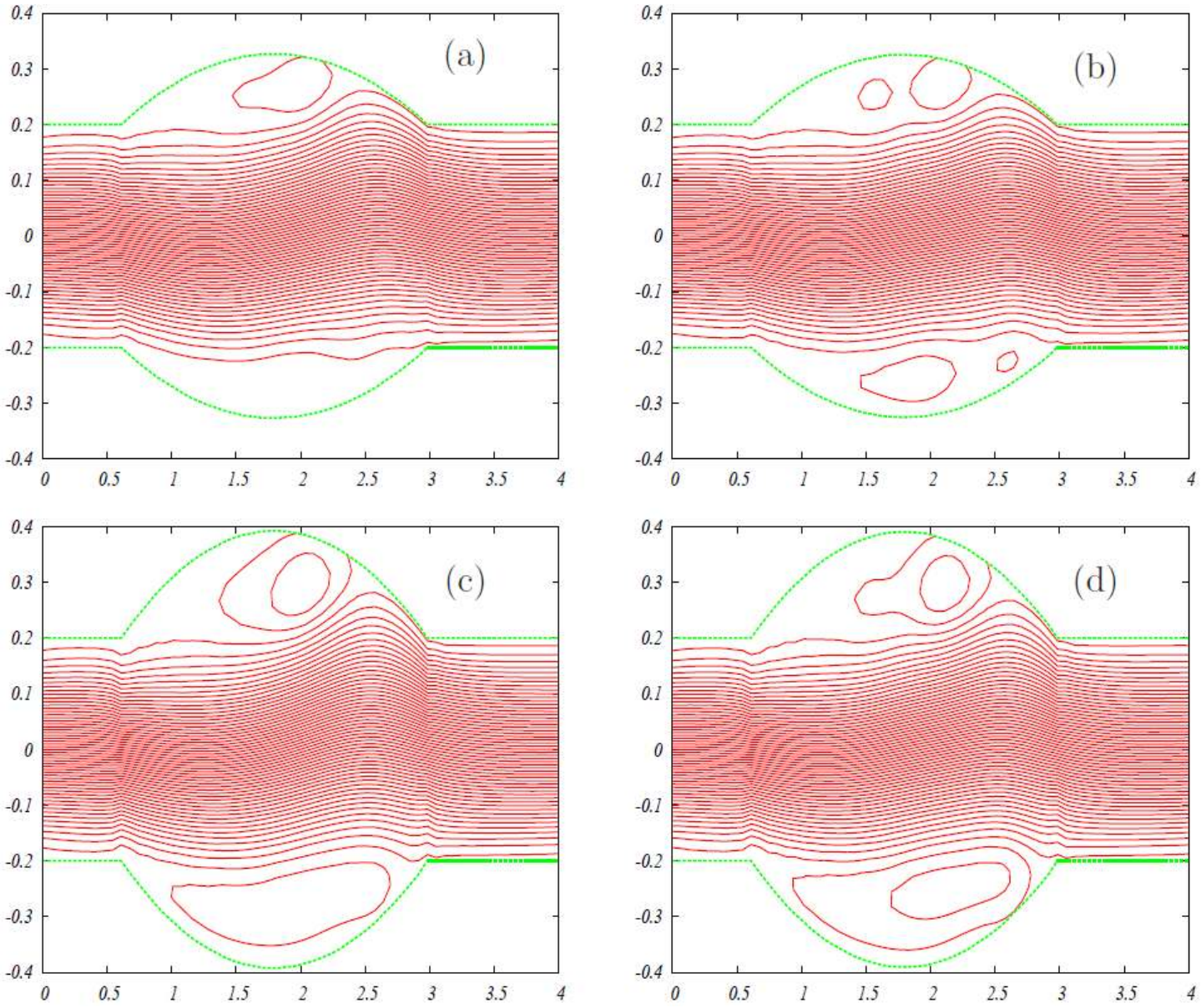

Figure 3: Streamlines obtained for for elastic wall and steady inlet flow for two aneurysms of different length. (a) and (b) transmural pressure to fluid density ratio equal 10. (a) Re = 2000, (b) Re = 3000. (c) and (d) transmural pressure to fluid density ratio equal 15. (a) Re = 1500, (b) Re = 2000.

The same features mentioned for a longer elastic wall, and shown in figure 6, exist here. That is the maximum expansion of the channel occurs at station (e) in the diastolic part of the cycle, the flow is asymmetric, the presence of two rolls located under the curved elastic wall and the rolls tend to disappear in the systolic part of the cycle as it is shown in figure 7. It is worthwhile to note that the presence of rolls under the curve wall invert the shear forces exerted by the flow on the wall which must be a dramatic event for the endothelial cells.

8 ANALYSIS OF THE SHELL MODEL USING A STEADY QUASI UNIFORM NON VISCOUS FLOW

In the previous section the spatial pressure variation is found to be very small in comparison to the mean pressure in the fluid. Therefore, the displacement of the wall is mainly due to the difference between the external pressure and the mean internal pressure and it is not very sensitive to spatial pressure fluctuations. The numerical experiments show that the local

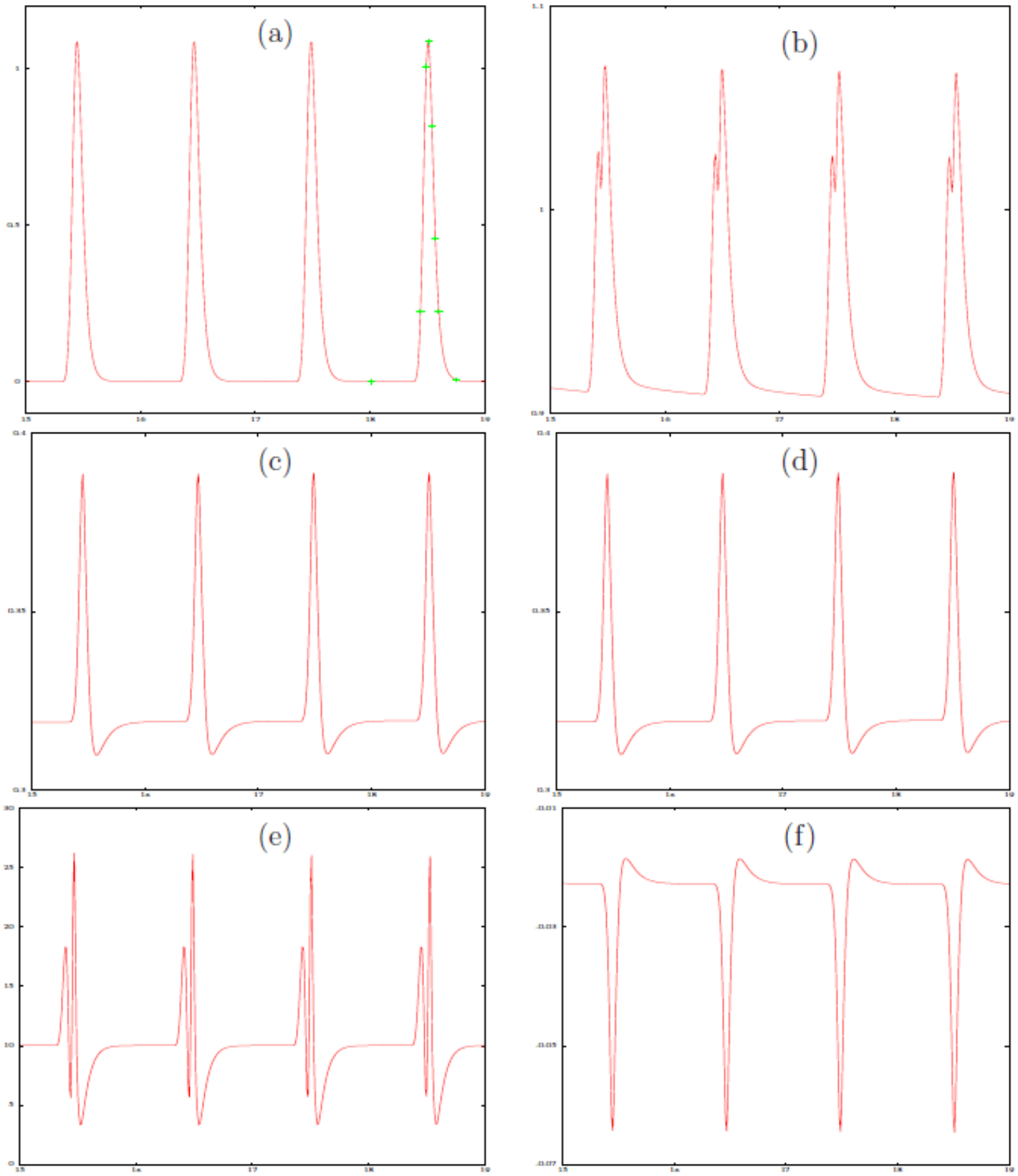

Figure 4: (a) The amplitude of pulse at the inlet of the channel versus time, (b) the axial velocity component at the middle of the channel versus time, (c) the displacement of the upper wall at the middle of elastic wall versus time, (d) the displacement of the lower wall at the middle of the elastic wall versus time , (e) the pressure at the middle of channel versus time and (f) the tension inside the wall at the middle of the channel versus time.

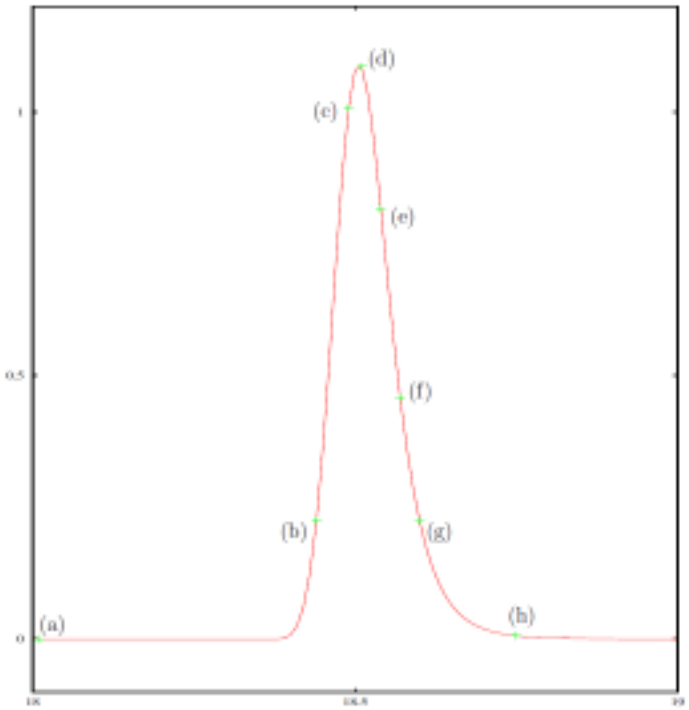

Figure 5: The pulse at the entrance of the channel versus time. The sign + indicates the stations where a sample of streamlines are plotted in this paper.

flow pressure variation has an insignificant effect on the movement of the wall. These findings suggest and support the analysis done in this section. In order to simplify the analysis, the displacement of the wall are assumed to be symmetric, therefore only the upper half of the channel shall be considered in this analysis. Let p_t be the head pressure at the entrance of the channel, then, in a steady inviscid flow, according to Bernoulli theorem, the inner pressure at an arbitrary cross-section of the channel is

$$p_t = p_i + \rho_f \frac{v^2}{2} \tag{42}$$

where p_i is the inner pressure, v is the uniform flow velocity in the cross-section S of the channel and ρ_f is the mass density of the fluid. In a steady uniform flow, the conservation of mass yields

$$Q = vS = v(h + u_2) \quad ; \quad v = \frac{Q}{h + u_2} \tag{43}$$

where Q is volume flux and $S = (h + u_2) \times$unity length in spanwise direction. Thus, the inner pressure is

$$p_i = p_t - \frac{\rho_f Q^2}{2h^2} \frac{1}{(1 + \frac{u_2}{h})^2} \tag{44}$$

The transmural pressure can be written as

$$\frac{p_e - p_i}{h} = \frac{p_e - p_t}{h} + \frac{\rho_f Q^2}{2h^3} \frac{1}{(1 + \frac{u_2}{h})^2} = C + \frac{C_1}{(1 + \frac{u_2}{h})^2} \tag{45}$$

where

$$C = \frac{p_e - p_t}{h} \quad ; \quad C_1 = \frac{\rho_f Q^2}{2h^3} \tag{46}$$

Let's define the new dimensionless variables

$$z = \frac{u_2}{h} \; ; \; x = \frac{a_1}{h} \; ; \; \phi = \frac{\mu}{hC} = \frac{\mu}{p_e - p_i} \tag{47}$$

and introduce the new parameters,

$$C_2 = \frac{C_1}{C} = \frac{\rho_f Q^2}{2h^2} \frac{1}{p_e - pi} = \frac{\rho_f Q^2}{2\mu h^2} \frac{\mu}{p_e - pi} = \frac{\rho_f Q^2}{2\mu h^2} \phi = \lambda^2 \phi \tag{48}$$

where

$$\lambda^2 = \frac{\rho_f Q^2}{2\mu h^2} \tag{49}$$

Using the precedent dimensionless variables, the dynamic equation becomes

$$(\phi - z + \frac{C_2}{1+z}) \frac{\partial^2 z}{\partial x^2} - [(\frac{\partial z}{\partial x})^2 + 1](1 + \frac{C_2}{(1+z)^2}) = 0 \tag{50}$$

The first integral of the above equation can be written as

$$(\phi - z + \frac{C_2}{1+z}) \frac{\partial^2 z}{\partial x^2} - [(\frac{\partial z}{\partial x})^2 + 1](1 + \frac{C_2}{(1+z)^2}) = 0 \tag{51}$$

where

$$\gamma_1 = \frac{1}{2}(\phi - 1 + \sqrt{\Delta}) \; ; \; \gamma_2 = \frac{1}{2}(\phi - 1 - \sqrt{\Delta})$$
$$\Delta = (1 - \phi)^2 + 4(\phi + C_2)$$

and β is a constant of integration. So, the solution of equation 50 can be obtained in the form of a quadrature:

$$\int \frac{(z - \gamma_1)(z - \gamma_2) dz}{\sqrt{\beta(z+1)^2 - [(z - \gamma_1)(z - \gamma_2)]^2}} = \pm x + K \tag{52}$$

which, after some algebra, can be written as

$$\int \frac{z^2 + (1 - \phi)z - \phi - C_2}{\sqrt{\beta(z+1)^2 - [z^2 + (1 - \phi)z - \phi - C_2]^2}} dz = \pm x + K \tag{53}$$

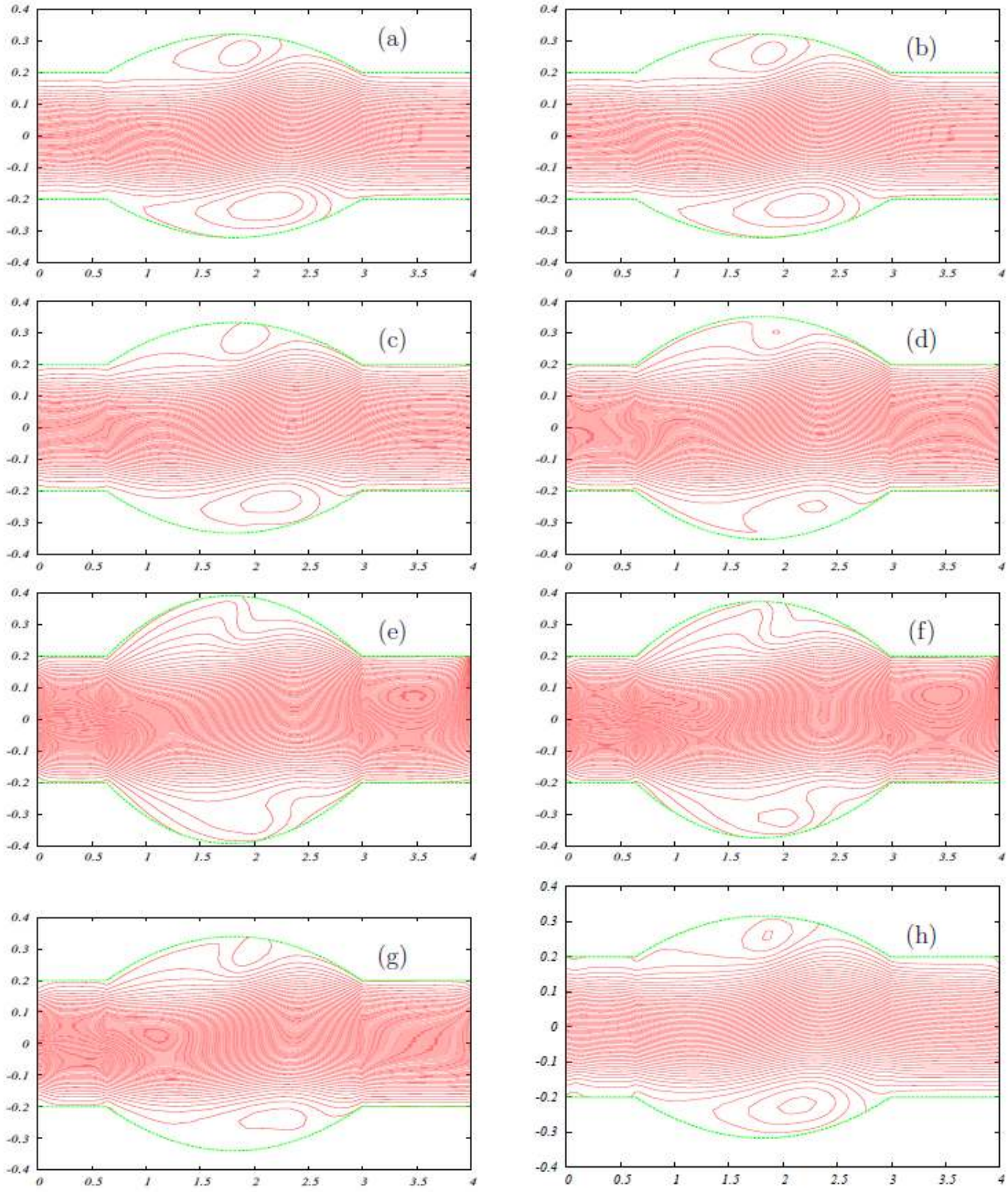

Figure 6: The streamlines for elastic wall and pulsatile inlet flow at some stations selected in a period as it is indicated in figure 5. Re = 2000, transmural pressure to fluid density ratio equal 10 m^2/s^2

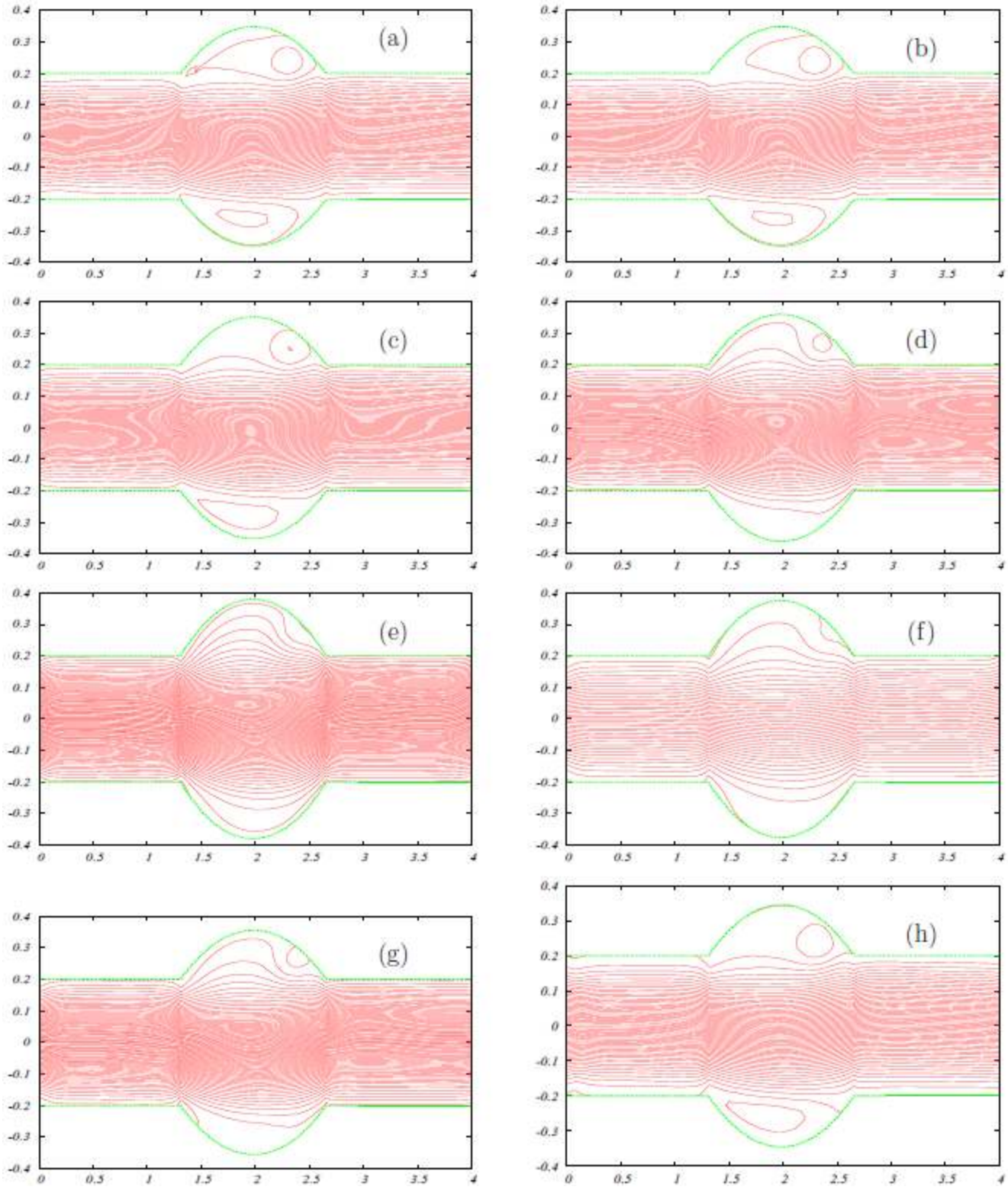

Figure 7: The streamlines for elastic wall and pulsatile inlet flow at some stations selected in a period as it is indicated in figure 5. Re = 2000, transmural pressure to fluid density ratio equal 15 m^2/s^2.

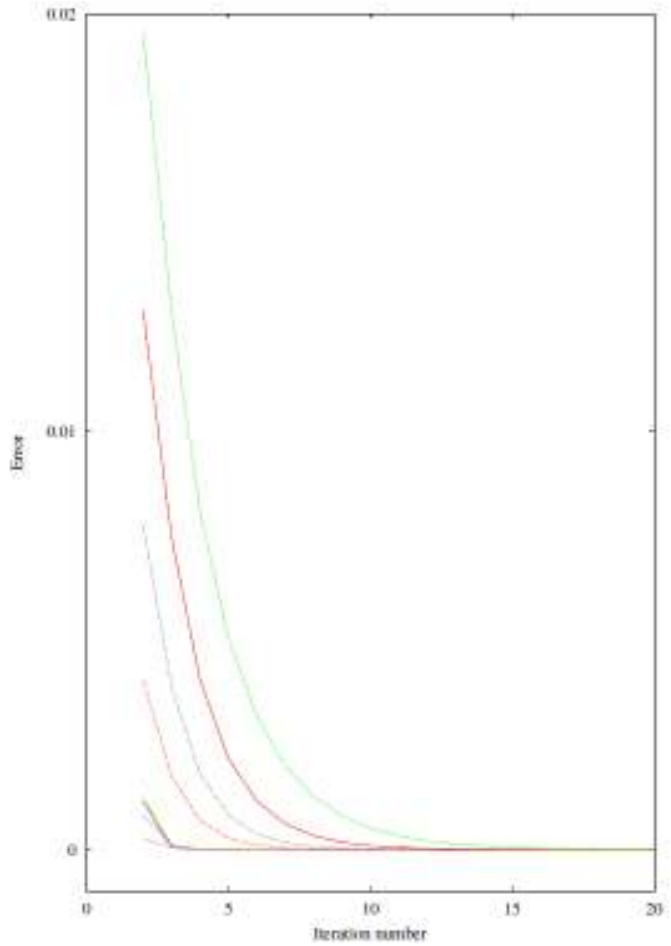

Figure 8: Convergence of the numerical iteration in solving integral equation. Equation 71. Error versus iteration number, from down to up, $\lambda^2 \in \{0.01, \dots, 0.11\}$_2 2 {0.01, · · · , 0.11}, dimensionless trans-mural pressure ϕ=-20. The error is difine as follow $Error = \left|\int_0^L (z_{n+1}^2 - z_n^2)dx\right|$

The two arbitrary constants β and K must be fixed by the boundary conditions.

9 PARTICULAR CASE WHERE $C_2 = 0$: THE PRESSURE VARIATION DUE TO THE FLOW VELOCITY IS DISREGARDED

For low flow rate i.e. $\lambda \ll \Phi$, the pressure variation due to the fluid velocity is small in comparison the transmurale pressure. In this case it is plausible to neglect the terms multiplied by C_2. In the limit of the approximation $C_2 \approx 0$, equation 53 becomes

$$\int \frac{(z-\phi)}{\sqrt{\beta-(z-\phi)^2}}dz = -\sqrt{\beta-(z-\phi)^2} = \pm x + K \qquad (54)$$

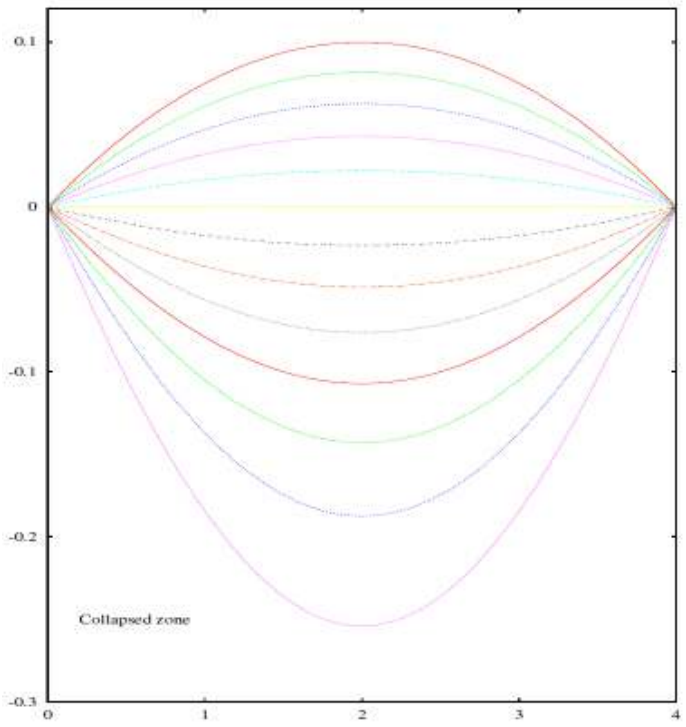

Figure 9: Form of the shell for some trasmural pressure

the boundary conditions $z(0) = 0$, $z(L) = 0$ specify the constants β and K so that

$$(z-\phi)^2 = \phi^2 + \frac{L^2}{4} - (\frac{L}{2} - x)^2 \qquad (55)$$

It is clear from this that the shell takes the form of portion of a circle centered at $\left(\frac{L}{2}, \Phi\right)$ and of radius $R = \sqrt{\Phi^2 + \frac{L^2}{4}}$. This is the well known fusiform shape of aneurysms.

10 SOLUTION IN THE FORM OF AN INTEGRAL EQUATION

Let's reconsider equation 51,

$$(\frac{dz}{dx})^2 + 1 = \beta(\frac{z+1}{(z-\gamma_1)(z-\gamma_2)})^2 = \frac{\beta}{H^2} \qquad (56)$$

where we introduced a new variable

$$H = \frac{(z-\gamma_1)(z-\gamma_2)}{z+1} \iff \dot{H} = \frac{dH}{dz} = (1 + \frac{\lambda^2\phi}{(z+1)^2}) \qquad (57)$$

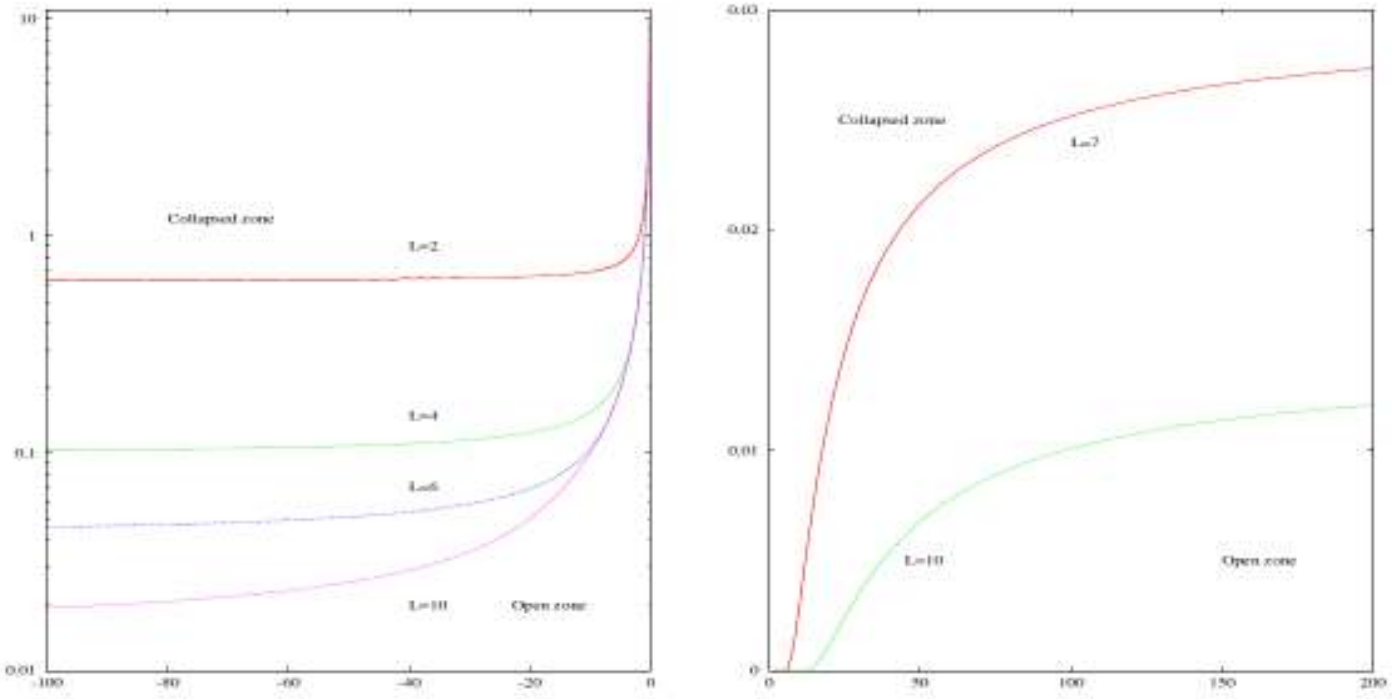

Figure 10: Limit zone where a steady solution has been found

Equation 56 can be written as

$$(\frac{\partial z}{\partial x})^2 = \frac{\beta - H^2}{H^2} \Longleftrightarrow \frac{H}{\sqrt{\beta - H^2}} dz = \pm dx \qquad (58)$$

Multiplication of by H yields

$$\frac{\dot{H}H}{\sqrt{\beta - H^2}} dz = \pm \dot{H} dx = \pm (1 + \frac{\lambda^2 \phi}{(z+1)^2}) dx \qquad (59)$$

By integration we have

$$-\sqrt{\beta - H^2} = \pm (x + \lambda^2 \phi \int_0^x \frac{dx}{(z+1)^2}) + K \qquad (60)$$

Henceforth, the term involving an integral shall be noted $I(x)$, that is

$$I(x) = \int_0^x \frac{dx}{(z+1)^2} \qquad (61)$$

With this notation, equation 60 becomes

$$-\sqrt{\beta - H^2} = \pm (x + \lambda^2 \phi I(x)) + K \qquad (62)$$

Squaring the precedent equation yields,

$$[\frac{(z-\gamma_1)(z-\gamma_2)}{z+1}]^2 = \beta - [\pm (x + \lambda^2 \phi I(x)) + K]^2 \qquad (63)$$

The boundary condition at $z(0) = 0$ and $z(L) = 0$ allow the elimination of the constant β and K, so that the solution becomes

$$[\frac{(z-\gamma_1)(z-\gamma_2)}{z+1}]^2 = (\frac{L + \lambda^2 \phi I(L)}{2})^2 \qquad (64)$$
$$+(\gamma_1 \gamma_2)^2 - [x + \lambda^2 \phi I(x) - \frac{L + \lambda^2 \phi I(L)}{2}]^2$$

Note that this is an integral equation as the term $I(x)$ depends on the solution z. Let's note the right-hand side by $F(x)$, that is

$$F(x) = (\frac{L + \lambda^2 \phi I(L)}{2})^2 + (\gamma_1 \gamma_2)^2 - [x + \lambda^2 \phi I(x) - \frac{L + \lambda^2 \phi I(L)}{2}]^2 \qquad (65)$$

Then, equation 64 becomes

$$(z-\gamma_1)(z-\gamma_2) = p_1 (z+1)\sqrt{F(x)} \qquad (66)$$

where p_1 stands for $\pm$. Substitution of γ_1 and γ_2 into the above equation yields

$$z^2 + (1-\phi)z - \phi(1+\lambda^2) = \pm (z+1)\sqrt{F(x)} = p_1 (z+1)\sqrt{F(x)} \qquad (67)$$

Notice that $F(0) = F(L) = \Phi^2 (1+\lambda^2)^2$. In order to enforce the boundary condition we have to chose p_1 according to the sign

of the term Φ, that is $p_1 = -sgn(\Phi)$. The solution of equation 67 reads

$$z = \frac{1}{2}\{-1+\phi-p_1\sqrt{F(x)}+ p_2\sqrt{[1-\phi+p_1\sqrt{F(x)}]^2+4[\phi+\lambda^2\phi-p_1\sqrt{F(x)}]}\} \quad (68)$$

where p_2 stands for $= \pm$ as

$$\sqrt{F(0)} = \sqrt{F(L)} = \sqrt{(\gamma_1\gamma_2)^2} = \mid \phi \mid (1+\lambda^2) \quad (69)$$

in order to enforce the boundary conditions at $x = 0$ and at $x = L$, we have to chose p_2 according to the sign of the term

$$T = -1+\phi+p_1\sqrt{F(0)} = -1+\phi+p_1\sqrt{F(L)} = -1+\phi+p_1\sqrt{[\phi(1+\lambda^2)]^2} \quad (70)$$

In order to keep the boundary condition being enforced we have to take

$$p_2 = -\mathrm{sgn}(-1+\phi+p_1\sqrt{[\phi(1+\lambda^2)]^2})$$

Thus, the solution becomes

$$z = \frac{1}{2}\{-1+\phi-p_1\sqrt{F(x)}+ p_2\sqrt{[1-\phi+p_1\sqrt{F(x)}]^2+4[\phi(1+\lambda^2)-p_1\sqrt{F(x)}]}\} \quad (71)$$

$$F(x) = (\frac{L+\lambda^2\phi I(L)}{2})^2 + [\phi(1+\lambda^2)]^2 - [x+\lambda^2\phi I(x) - \frac{L+\lambda^2\phi I(L)}{2}]^2 \quad (72)$$

$$I(x) = \int_0^x \frac{dx}{(z+1)^2} \quad (73)$$

$$p_2 = -\mathrm{sgn}(-1+\phi+p_1\sqrt{[\phi(1+\lambda^2)]^2}) \quad (74)$$

where

$$\phi = \frac{\mu}{p_e - p_t} \;\; ; \;\; \lambda^2 = \frac{\rho Q^2}{2\mu h^2} \quad (75)$$

As the right hand side of equation 71 involves the solution z, via the function $F(x)$ defined in equation 72, an iterative method is required to solve for z. Figure 8 shows how the error decreases with the number of iteration. For low transmural pressure to mass density ratio, the numerical method requires only a few iterations. However, the number of iterations increases with transmural pressure to not converge at all for very large transmural pressures. However, it is not clear whether the divergence occurs because the steady solution does not exist or simply because the numerical procedure becomes unstable for large transmural pressure. Figure 8 shows the form of the upper shell negative transmural pressure. The used numerical procedure does not converge in the zone marked as "Collapsed zone".

11 CONCLUSION

Vibrations induced by flow and elastic wall interaction arise in many energetic applications, after a review of some important examples in fluid-structure interaction, the paper addresses the flow and wall interaction in an abnormally deformed arteries, phenomenon known as aneurysm. A simplified nonlinear integral-partial-differential equation is devised to describe the aneurysm's wall dynamic. In order to handle large displacements and large deformations, Lagrangian variables are used. In some interesting particular cases a formal solution of the nonlinear integral-partial-differential equation governing the wall motion is found. In peculiar, the obtained solution shows that the form of the wall under a constant transmural pressure is an arc of a circle. A first integral of the wall equation is derived for quasi uniform inviscid flow velocity, i.e, for the cases where the axial velocity component is much larger than the spanwise velocity component.

A numerical simulation taking into account a full coupling between the wall and the flow inside the aneurysm has been presented. The wall motion is described by the above mentioned integral-partial-differential equation written in Lagrangian form, and the flow is described by the two dimensions Navier-Stokes equations. Three categories of numerical experiments are done here. In the first experiment the curve aneurysm wall is fixed (supposed to be rigid) and the inlet flow is steady. It is found that the flow in this case is steady, and that for both Reynolds number $Re = 1500$ and $Re = 2000$ it is found that two quasi symmetric counter rotating rolls appear under the curve aneurysm walls, inverting the direction of the shear stress at the interface fluid/solid.

The second experiment used a steady inlet flow and elastic wall, i.e the wall allowed is to move under the variation of transmural pressure over time. It is found that the flow is asymmetric in this case. The flow is found to be unsteady for

$Re = 2000$ and $Re = 3000$ and transmural pressure to density ratio $\frac{\Delta p}{\rho} = 10 m^2/s^2$, as well as for $Re = 1500$, $Re = 200$ and transmural pressure to density ratio $\frac{\Delta p}{\rho} = 15\ m^2/s^2$. However, the wall displacement and the variation of the streamlines of the flow over time are very small. Two asymmetric rolls appear under the curve aneurysm wall, which inverts the direction of the shear stress exerted by the flow on the wall. As the symmetry is broken in this case, it is inferred that the friction forces in the vicinity of the walls must be of different amplitude which could lead to asymmetric evolution of the aneurysm shape over a long period.

The third experiment is for a periodic pulsatile flow at the inlet of the channel and a curve elastic wall. After a long period, when the effects of the initial conditions have been diminished, the flow becomes quasi periodic. Samples, in six stations in the laps of one period, are taken to examine the flow. Two sub cases are considered: in the first, a relatively long aneurysm subjected to a relatively low transmural pressure to density ratio is considered. In the second, a relatively short aneurysm subjected to a relatively high transmural pressure to density ratio is considered. In both cases the flow obtained by numerical simulation is asymmetric. The presence of two rolls under the curve walls is confirmed in these cases too. However, during the systolic period, the rolls are virtually removed and the flow tends to be unidirectional. An interesting feature of the pulsatile flow which appears in the present experiments is that there is a gap between the instant where the inlet rate flow reaches its maximum and the instant where the maximum expansion of the wall occurs, i.e, the maximum of the inlet flow and the maximum of walls displacement do not occur simultaneously.

It is commonly accepted that, in arteries, at the interface fluid/solid, there exists a thin layer, the intima, which contains the so called endothelial cells that are sensitive to flow induced shear stress and pressure. The endothelial cells seem to be able to exercise a sort of active control, where the sensors are the mechanical parameters (friction and pressure), and the actuators are a kind of vasodilators enzymes, which are able to modify the rheological parameters of the arteries tissues, allowing them to expand or to narrow accordingly and to change the elastin to collagen fiber ratio in wall composition. The present work presents a methodical approach to compute the shear stress exerted by the flow on the endothelial cells, which is a necessary step in modeling long term evolution of the aneurysm.

To the best of the author's knowledges, nowadays, there is no mathematical model which involves a coupling between biological factors and mechanical factors at short and long time scales. The achievement of this model could lead to insight in the creation and the development of aneurysms and likely predicts its rupture. The present studies give insight on the interaction between the flow and the elastic wall of aneurysms at short time scale which constitutes a good step towards a more general model that accounts for all time scales in modeling the aneurysm development.

REFERENCES

[1] Lasheras, J. C. 2010 Haemodynamic stresses and the onset and progression of vascular diseases. J. Fluid Mech. 664, 1-4.

[2] Lasheras, J. C. 2007 The biomechanics of arterial aneurysms. Annu. Rev. Fluid Mech. 39, 293-319.

[3] Duclaux, V., Gallaire, F. & Clanet, Ch. 2010 A fluid mechanical view on abdominal aortic aneurysms. J. Fluid Mech. 664, 5-32.

[4] Hamadiche, M., Scot, J. & Jeandel, D. 1994 Temporal stability of Jeffery-Hamel flow. J. Fluid Mech. 268, 71-88.

[5] Fung, Y. C. 1990 Biomechanics. Motion, Flow, Stress and Growth. Springer-Verlag, New York.

[6] Humphrey, J. D. 1995 Mechanics of the Arterial Wall: Review and Directions. Crit. Rev. Biomed. Eng. 23, 1-162.

[7] Holzapfel, G. A., Gasser, Th. C. & Ogden, R. W. 2004 Comparison of a Multi-Layer Structural Model for Arterial Walls With a Fung-Type Model, and Issues of Material Stability. Transactions ASME. 126(4), 264-275.

[8] Sheidaei, A., Hunley, S. C., Zeinali-Davarani, S., Raguin, L. G. & Baek S. 2011 Simulation of abdominal aortic aneurysm growth with updating hemodynamic loads using a realistic geometry. medical Engineering & physics. 33, 80-90.

[9] Figueroa, C. A., Baek, S., Taylor, C. A. & Humphrey J. D. 2009 A computational framework for fluid-solid-growth modeling in cardiovascular simulations. Computer Methods in Applied Mechanics and Engineering. 198 3583-3602.

[10] Bertram, C. D. & Castles, R. J. 1999 Flow limitation in uniform thick-walled collapsible tubes. International Journal of Solids and Structures. 13, 399-418.

[11] Duvaut, G. 1998 Mécanique des milieux continus. Dunod, Paris.

[12] Hamadiche, M., Kizilova, N. & Gad-el-Hak, M. 2009 Suppression of Absolute Instabilities in the Flow Inside a Compliant Tube. Communications in Numerical Methods in Engineering. 25, 505-531.

[13] Hamadiche, M. & Gad-el-Hak, M. 2004 Spatiotemporal Stability of Flow through Collapsible, viscoelastic tubes. AIAA journal. 42, No. 4, 772-786.

[14] Hamadiche, M. & Gad-el-Hak, M. 2002 Temporal Stability of Flow through Viscoelastic Tubes. Journal of Fluids and Structures. 16, No 3, 331-359.

[15] Olivier Doaré and E ; de Langre The flow-induced instability of long hanging pipes,Europen Journal of Mechanics A/Solide Volume 21, 2002, Pages 857-867

[16] Hamadiche, M. and Abu Shadi, H. 2006 Flow induced vibration during the optic fiber coating process. Journal Fluid and Structure, Vol. 22(5), p. 599-615.
[17] B. H. Tan, A.D. Lucey and R. M. Howell Aero-/hydro-elastic stability of flexible panels: Prediction and control using localised spring support, Journal of Sound and Vibration Volume 332, Issue 26, 23 December 2013, Pages 7033-7054
[18] Whittaker, J. R., Heil, M., Jensen, O. E. & Waters, W. L. 2010 Predicting the onset of high-frequency self-excited oscillations in elastic-walled tubes. Proc. R. Soc. 466, 3635-3657.